https://doi.org/10.5194/cp-2022-67
Preprint. Discussion started: 6 September 2022

Climate of the Past
Discussions
Open Access

Deglacial records of terrigenous organic matter accumulation off the Yukon and Amur rivers based on lignin phenols and long-chain *n*-alkanes

Mengli Cao[1], Jens Hefter[1], Ralf Tiedemann[1,2], Lester Lembke-Jene[1], Vera D. Meyer[3], Gesine Mollenhauer[1,2,3]

[1]Alfred-Wegener-Institut, Helmholtz-Zentrum für Polar-und Meeresforschung (AWI), 27570 Bremerhaven, Germany.
[2]Department of Geosciences, University of Bremen, 28359 Bremen, Germany.
[3]MARUM-Center for Marine Environmental Sciences, University of Bremen, 28359 Bremen, Germany.

Corresponding author:
Mengli Cao, mengli.cao@awi.de
Gesine Mollenhauer, gesine.mollenhauer@awi.de

Abstract:

Arctic warming and sea level change will lead to widespread permafrost thaw and subsequent mobilization. Sedimentary records of past warming events during the last glacial–interglacial transition can be used to study the conditions under which permafrost mobilization occurs. Long-chain *n*-alkyl lipids and lignin phenols are two types of biomarkers excellently suited for the reconstruction of terrestrial higher plant vegetation, as they are derived from epicuticular waxes and from the major rigidifying material of higher plants. For the Okhotsk and Bering Seas off the mouths of the Amur and Yukon rivers, respectively, published records reported the temporal variations of *n*-alkyl lipid accumulation recording mostly erosive processes. Surface runoff, vegetation type, and degree of organic matter degradation as reflected by lignin have not been investigated so far.

Here, we present new lignin phenol records from marine sediment cores and compare them with previously published lipid biomarker data from these two subarctic marginal seas. We find that in the Yukon Basin, vegetation change and wetland expansion began already in the early deglaciation (ED, 14.6–19 ka BP). This timing is different from observed changes in the Okhotsk Sea reflecting input from the Amur Basin, where wetland expansion and vegetation change occurred later in the Preboreal (PB). In the two basins, angiosperms contribution and wetland extent all reached maxima during the PB, both decreasing and stabilizing after the PB. We also find that the permafrost of the Amur Basin began to become remobilized in the PB. Retreat of sea-ice coupled with increased sea-surface temperatures in the Bering Sea

https://doi.org/10.5194/cp-2022-67
Preprint. Discussion started: 6 September 2022

Climate of the Past
Discussions

during the ED might have promoted early permafrost mobilization. In both records, accumulation rates of lignin phenols and lipids are similar, suggesting that under conditions of rapid sea-level rise and shelf flooding, both types of terrestrial biomarkers are delivered by the same transport pathway.

1. Introduction

Climate warming caused by anthropogenic perturbation affects the Arctic more strongly than other regions of the world. Warming climate induces environmental changes that accelerate degradation of organic matter (OM) stored in permafrost and promote greenhouse gas release (Schuur et al., 2015). Permafrost, or permanently frozen ground, is soil, sediment, or rock that remains at or below 0 °C for at least two consecutive years. It occurs both on land and beneath offshore arctic continental shelves, and underlies about 22 % of the Earth's land surface (Brown et al., 2002). Most of today´s circum-arctic permafrost deposits in the Yedoma region of Siberia and Alaska developed under continental cold climate conditions in unglaciated regions during the late Pleistocene (Strauss et al., 2021). Across the northern circum-polar permafrost regions, Yedoma deposits, 0–3 m soils and deltas contain about twice as much carbon as the pre-industrial atmospheric carbon pool (Hugelius et al., 2014).

During the deglacial and Holocene warming ground ice melted, causing the land surface to collapse into space previously occupied by ice wedges, a process called thermokarst. This led to the formation of thermokarst lakes and thermo-erosional valleys as well as rivers, and also likely the release of carbon from thawed deposits (Walter et al., 2006; Walter Anthony et al., 2014). Around 70 % of the Yedoma region thawed beneath thermokarst lakes and streams since 14.7 ka BP (Walter Anthony et al., 2014). Based on a carbon cycle model, Köhler et al. (2014) suggested that deglacial thawing of permafrost in the Northern Hemisphere at the onset of the Bølling/Allerød (B/A) may have caused an abrupt CO_2 rise and a drop in atmospheric $\Delta^{14}C$, with a possible contribution from flooding of the Siberian continental shelf during melt water pulse 1A (MWP-1A).

During millennia following the formation of thermokarst lakes, mosses and other plants grew in and around them, which may in part have offset permafrost carbon release (Walter Anthony et al., 2014; Schuur et al., 2015; Turetsky et al., 2020). *Alnus* is a common genus in Yukon Holocene pollen records but far less common in interglacials, because *Alnus* groves frequently develop along newly formed local

https://doi.org/10.5194/cp-2022-67
Preprint. Discussion started: 6 September 2022

drainage features linked to permafrost degradation (Schweger et al., 2011). Several studies suggested major deglacial changes in the vegetation of permafrost-affected areas during the last deglaciation, including the Yukon Territory (Fritz et al., 2012), Sakhalin peninsula and Hokkaido (Igarashi and Zharov, 2011), the Lena River basin (Tesi et al., 2016), and the Amur River basin (Seki et al., 2012).

Biomarker compositions, distributions and contents in marine sediments can help to elucidate the processes responsible for terrestrial OM export from land and the fate of this OM in the ocean. Long-chain *n*-alkyl lipids and lignin phenols are two types of biomarkers commonly used to reconstruct supply of terrigenous OM to the ocean. While long-chain *n*-alkyl lipids with a strong predominance of the odd carbon number homologues derive from the epicuticular waxes of vascular and aquatic plants (Eglinton and Hamilton, 1967), the latter are constituents of the lignin polymer, which constitutes up to one third of all woody material of living plants (Erdtman, 1971). The *n*-alkanes (Alk) likely trace terrigenous OM which has been mobilized from thawing permafrost deposits (Feng et al., 2013) and may be transported into the marine sediment primarily following coastal erosion during shelf flooding (Winterfeld et al., 2018). In contrast, lignin is transported from land to sea via different conduits than *n*-alkane biomarkers (Feng et al., 2013) and has the potential to provide information on surface runoff processes and wetland extent (Tesi et al., 2016; Feng et al., 2015). In addition, lignin reflects the type of vegetation and the degree of OM degradation (Hedges and Mann, 1979; Hedges et al., 1988). According to lignin phenols and the so-called branched and isoprenoid tetraether index (BIT), Seki et al. (2014) found that terrestrial OM from the Amur River is a major source of OM in the North Pacific Ocean at present and that terrestrial OM in surface sediments is dominated by gymnosperms in the Okhotsk Sea. So far, no records exist that combine both types of terrigenous biomarker data to explore the potentially different transport histories of terrestrial OM archived in them.

In this study, we present downcore records of lignin phenols from the early deglaciation to the early Holocene from two contrasting river-dominated continental margin sites in the North Pacific area. We interpret the lignin phenol records in context of vegetation and wetland development and investigate the temporal evolution of the different pathways of terrigenous OM export to the ocean by comparing the two types of terrigenous biomarkers, i.e., Alk and lignin phenols.

https://doi.org/10.5194/cp-2022-67
Preprint. Discussion started: 6 September 2022

2. Study area

The Bering Sea is located in the north of the Pacific Ocean. The Yukon River is the fourth largest river in North America in terms of annual discharge, and drains into the Bering Sea (Holmes et al., 2012). The deglacial sediments from the Bering Sea contain records both of sea-level rise-induced erosion of the vast Bering Shelf, and of runoff from the Yukon River (Kennedy et al., 2010; Meyer et al., 2019). The Yukon Basin was mostly unglaciated during the LGM, featuring permafrost (Schirrmeister et al., 2013; Meyer et al., 2019), and remains mostly so until today. Arctic coasts today often are eroded at high rates of up to several meters per year (Lantuit et al., 2011; Couture et al., 2018), suggesting that during past periods of sea-level rise, similar or even stronger erosive forces were at play supplying vast amounts of terrigenous materials to marine sediments. Today the catchment of the Yukon River is covered by spruce forest (20 %), grassland (40 %), shrubland (20 %), and open water and wetlands associated with the lowland areas (8 %) (Amon et al., 2012). Pollen records indicate there were no significant changes in vegetation pattern from the LGM to about 16 ka BP, but after about 16 ka BP, birch pollen became significantly more abundant from western Alaska to the Mackenzie River (Bigelow, 2013). In the early Holocene, significant Populus-Salix woodland development occurred in interior Alaska and in the Yukon Territory (Bigelow, 2013).

The Okhotsk Sea, a semi-enclosed marginal sea located in the west of the North Pacific, is known as the southernmost region of seasonal sea ice in the Northern Hemisphere today. The continental slope off Sakhalin Island in the Okhotsk Sea receives runoff from the Amur river, which is one of the largest rivers in the world in terms of the annual total output of dissolved OM (Nakatsuka et al., 2004) and substantially influences the formation of seasonal sea ice (Nakatsuka et al., 2004). The catchment of the Amur transitioned from complete permafrost coverage during the LGM to almost entirely permafrost-free conditions at present (Vandenberghe et al., 2012). The climate of the Amur Basin is largely determined by continental patterns from Asia, while monsoon influences from the Pacific transport precipitation to this region during the summer. Previous studies found that herbaceous plants were the predominant vegetation in the last glacial periods in the Amur Basin, and were replaced by gymnosperms during the deglaciation and Holocene (Bazarova et al., 2008; Seki et al., 2012). The vegetation of the Amur Basin belongs mostly to the

https://doi.org/10.5194/cp-2022-67
Preprint. Discussion started: 6 September 2022

Taiga zone, with larch as the most common species in the area. The upper reaches of the Amur Basin belong to the coniferous continental taiga at present. The central areas are dominated by mixed coniferous and broad-leaved forests and the coniferous larch forests are the predominant vegetation in the lower Amur Basin.

3. Material and methods

3.1. Sampling and age control

Piston core SO202-18-3 (60.13° N, 179.44° W, water depth: 1111 m) and neighboring Kasten core SO202-18-6 (60.13° N, 179.44° W, water depth: 1107 m) were recovered from the northeastern continental slope of the Bering Sea in 2009 during R/V Sonne cruise SO202-INOPEX (Gersonde, 2012). The two cores can be treated as one composite record according to their ultrahigh-resolution micro-X-ray-fluorescence data, sediment facies analysis of laminae and radiocarbon dating results (Kuehn et al., 2014). It represents an apparently continuous sedimentary sequence dated back to the Last Glacial (~25 ka BP) (Kuehn et al., 2014). Selected samples from core SO202-18-6 (n = 20, 10–589 cm core depth, 6.23–12.65 ka BP) and from core SO202-18-3 (n = 29, 447–1423 cm core depth, 12.99–24.1 ka BP) with an average temporal resolution of ~510 years were analyzed for lignin-derived phenol contents.

The 23.7 m-long piston core SO178-13-6 (52.73° N, 144.71° E) was collected from the Sakhalin margin in the Okhotsk Sea during the expedition SO178-KOMEX with R/V Sonne (Dullo et al., 2004) (Fig. 1) with the lowermost interval corresponding to ~17.5 ka (Max et al., 2014). Selected samples (n = 51, 100–2340 cm core depth, 1.11–17.27 ka BP) from core SO178-13-6 were analyzed for lignin-derived phenol contents with an average temporal resolution of ~340 years.

Radiocarbon-based age models for the two cores are from Kuehn et al. (2014) for core SO202-18-3/6 and Lembke-Jene et al. (2017) for core SO178-13-6. The time interval covered by the records will be subdivided into five intervals, the early deglaciation (ED; 19–14.6 ka BP), the B/A (14.6–12.9 ka BP), the Younger Dryas (YD; 12.9–11.5 ka BP), the Pre-Boreal (PB, 11.5–9 ka BP) and the Holocene (＜9 ka BP).

3.2. Laboratory analyses

The extraction of lignin phenols was carried out based on the method of Goñi and Montgomery (2000a) and as described in Sun et al. (2017). Dried samples were oxidized with CuO (~500 mg) and ~50 mg ferrous ammonium sulfate in 12.5 ml 2N

NaOH under anoxic conditions. The oxidation was conducted with a CEM MARS5 microwave accelerated reaction system at 150 °C for 90 min. After oxidation, known amounts of recovery standards (ethyl vanillin and trans-cinnamic acid) were added to the oxidation products. The alkaline supernatant was acidified to pH 1 with 37 % HCl. The reaction products were subsequently recovered by two successive extractions with ethyl acetate. The combined ethyl acetate extracts were evaporated under a stream of nitrogen, then re-dissolved in 400 µl pyridine. Prior to injection into the gas chromatograph-mass spectrometer (GC-MS), an aliquot (30 µl) was derivatized with 30 µl bis-trimethylsily-trifluoroacetamide (BSTFA) + 1 % trimethylchlorosilane (TMCS) (55 ℃, 30 min). An Agilent 6850 GC coupled to an Agilent 5975C VL MSD quadrupole MS operating in electron impact ionization (70 eV) and full-scan (m/z 50–600) mode was used for analysis. The source temperature of the MS was set to 230 °C and the quadrupole to 150 °C. The GC was equipped with a DB-1 MS column (30 m × 0.25 mm i.d., film thickness 0.25 µm). Helium was used as carrier gas at a constant flow rate of 1.2 ml min^{-1}. Samples were injected in splitless mode in a split/splitless injector (S/SL) held at 280 °C. The temperature of the GC-MS column was programmed from 100 °C (initially held for 8 min.), ramped by 4 °C min^{-1} to 220 °C, then by 10 °C min^{-1} to 300°C with a final hold time of 5 min.

Eight lignin-derived phenols were analyzed in this study. They can be classified into three groups according to their plant sources and structures:

1. Vanillyl phenols (V) consisting of vanillin (Vl), acetovanillone (Vn) and vanillic acid (Vd).

2. Syringyl phenols (S), comprising syringealdehyde (Sl), acetosyringone (Sn) and syringic acid (Sd).

3. Cinnamyl phenols (C) that include *p*-coumaric acid (*p*-Cd) and ferulic acid (Fd). Besides, we also included some other oxidation products that do not necessarily originate from lignin, such as 3,5-dihydroxybenzoic acid (3,5Bd) and para-hydroxybenzenes (P) like *p*-hydroxybenzaldehyde (Pl), *p*-hydroxybenzophenone (Pn), and *p*-hydroxybenzoic acid (Pd).

These compounds were identified based on retention time and mass spectra. Quantification was achieved by peak areas of the respective compounds and using individual 5-point response factor equations obtained from mixtures of commercially available standards analyzed periodically. The yields of Pl, Vl and Sl were corrected

https://doi.org/10.5194/cp-2022-67
Preprint. Discussion started: 6 September 2022

by the recovery rate of ethyl vanillin and the recovery rate of trans-cinnamic acid was applied to correct the yield of other lignin-derived compounds and 3,5Bd (Goñi et al., 2000a, b). The standard deviation was determined from repeated measurements of a laboratory internal standard sediment extract (*n* = 12) and for the carbon-normalized concentration of the sum of 8 lignin phenols (Λ8, mg 100mg^{-1} OC) equals 0.31.

Mass accumulation rates (MAR) of vascular plant-derived lignin phenols were calculated as follows:

$$\text{sediment MAR expressed in g cm}^{-2}\text{ a}^{-1} = \text{sedimentation rate (cm a}^{-1}) \times \text{dry bulk density (g cm}^{-3})$$

$$\text{lignin MAR expressed in } \mu\text{g cm}^{-2}\text{ a}^{-1} = (\text{sediment MAR} \times \Sigma 8) \div 100$$

Σ8 represents the lignin content in mg 10g^{-1} dry sediment.

Lignin MAR were compared to published Alk MAR from the Okhotsk Sea (Winterfeld et al., 2018) and the Bering Sea (Meyer et al., 2019). The high molecular weight (HMW) Alk quantified for the Okhotsk Sea sediment core are C_{27}, C_{29}, C_{31} and C_{33} (Winterfeld et al., 2018). In the Bering Sea sediment core are, C_{23}, C_{25}, C_{27}, C_{29}, C_{31} and C_{33} Alk were quantified (Meyer et al., 2019).

Alkanes also have been shown to provide a second marker for wetland extent via the Paq index (Ficken et al., 2000). It represents the relative proportion of mid-chain length Alk (C_{23} and C_{25}) to long-chain Alk (C_{29} and C_{31}):

$$\text{Paq} = (C_{23}+C_{25}) / (C_{23}+C_{25}+C_{29}+C_{31})$$

From the polar fractions of the lipid extracts used by Meyer et al. (2019) for the Alk analyses, the abundances of isoprenoid glycerol dialkyl glycerol tetraethers (isoGDGTs) were determined using the methodology described in Meyer et al. (2016). The average temporal resolution is approximately 390 years. Briefly, 5 g freeze-dried sediment samples and 10 µg C_{46}-GDGT (internal standard) were extracted with an accelerated solvent extractor using 22 ml cells and dichloromethane:methanol = 9:1 (vol/vol) as solvent at 100 °C and 6.895E+6 Pa with 3 cycles of 5 min each. Then the extracts were dried by a rotary evaporator. After being dried, the extracts were hydrolyzed with 0.1 N potassium hydroxide in methanol:H_2O = 9:1 (vol/vol) and the neutral compounds were extracted with *n*-hexane. Different compound classes were separated by deactivated SiO_2 column chromatography. Polar compounds (including GDGTs) were eluted with methanol:dichloromethane = 1:1 (vol/vol). Afterward they were dissolved in hexane:isopropanol = 99:1 (vol/vol) and filtered with a

https://doi.org/10.5194/cp-2022-67
Preprint. Discussion started: 6 September 2022

polytetrafluoroethylene filter (0.45 μm pore size). Samples were brought to a concentration of 2 μg μl^{-1} prior to GDGT analysis. GDGTs were analyzed by high-performance liquid chromatography and a single quadrupole mass spectrometer (see Meyer et al. (2017) for more details). The relative abundances of isoGDGTs can be expressed as the TEX_{86}^{L} index (Tetra Ether index) which quantifies the relative abundance of isoGDGTs consisting of 86 C-atoms and can be used as a sea surface temperature (SST) proxy in settings where SST is below 15 °C (Kim et al. 2010). The regional calibration of SST and TEX_{86}^{L} is based on Seki et al. (2014).

$$TEX_{86}^{L} = \log(\text{GDGT-2}/(\text{GDGT-1}+\text{GDGT-2}+\text{GDGT-3}))$$

$$SST/°C = 27.2 \times TEX_{86}^{L} + 21.8$$

4. Results

4.1. Lignin concentrations and MARs

Lignin phenol concentrations were 0.19–1.43 mg 100mg^{-1} OC (Λ8) or 0.20–1.07 mg 10g^{-1} sediment (Σ8) in the Bering Sea sediments and 0.32–1.29 mg 100mg^{-1} OC or 0.40–2.16 mg 10g^{-1} sediment in the Okhotsk Sea record. Overall, the MAR of lignin is lower in the Bering Sea than in the Okhotsk Sea (Fig. 2c, d). During the ED, the lignin MAR began to increase in the Bering Sea sediment and kept increasing until it reached a maximum (17.70 μg cm^{-2} a^{-1}) at the B/A-YD transition (Fig. 2c). After the B/A, the lignin MAR started to decrease in the Bering Sea until the onset of the YD. The lignin MAR in the Bering Sea reached a more pronounced but short maximum (20.61 μg cm^{-2} a^{-1}) at the YD-PB transition, followed by a decrease to the Holocene. The lignin MAR in the Okhotsk Sea is more variable than in the Bering Sea record (Fig. 2d). The lignin MAR shows an initial maximum in the B/A, but reaches a more pronounced second peak (31.16 μg cm^{-2} a^{-1}) in the early PB. Similar to the Bering Sea, the lignin MAR decreased after about 11 3ka BP and into the Holocene, however, the lignin MAR in the Okhotsk Sea sediment featured a rather broad maximum between B/A and early Holocene.

Deglacial changes in the MARs of long-chain Alk have previously been reported for the same cores (Meyer et al., 2019; Winterfeld et al., 2018). The MAR of lignin and Alk changed mostly synchronously in the Bering Sea, but in the Okhotsk Sea, the increase in lignin MAR occurred later than in Alk MAR, and notably also later than in the Bering Sea (Fig. 2c, d). Alk MAR in the Okhotsk Sea featured two similar maxima in the B/A and during the YD-PB transition, while the lignin MAR maximum

https://doi.org/10.5194/cp-2022-67
Preprint. Discussion started: 6 September 2022

in the B/A is less pronounced than that at the YD-PB transition. Lignin MAR are more variable than Alk MARs between 10 and 7.8 ka BP.

4.2. Lignin source and degradation indicators

The S/V and C/V ratios yielded values of 0.36–0.86 and 0.11–0.46 in the Bering Sea (Fig. 3, Ia, b), while slightly higher ratios of 0.41–0.92 and 0.19–0.70 were obtained in the Okhotsk Sea (Fig. 3, IIa, b). The standard deviations for S/V and C/V are 0.08 and 0.10, respectively. In the Bering Sea, the S/V ratios began to increase from 18 ka BP and kept increasing until it reached a maximum in the transition of the YD to the PB. The change of C/V values was not as obvious as S/V values, but it also reached its maximum at YD-PB transition. Subsequently, S/V and C/V ratios decreased during the Holocene and reached minima at the top of the core.

In the Okhotsk Sea, the S/V values increase slowly from the ED to PB, but the C/V ratios do not display an obvious increase over the same time, except for a maximum in C/V ratios around 15 ka BP. Minimum values were found in the ED and values remained rather low before the YD-PB transition. After reaching maxima in the PB, S/V and C/V ratios decreased during the Holocene, stabilizing at a higher level than during the ED.

In the Bering Sea, the 3,5Bd/V ratio ranged from 0.09 to 0.20 (Fig. 3, Id) (standard deviation: 0.02). From the end of LGM to the YD, the 3,5Bd/V ratio decreased slowly, but began to increase and reached a small local maximum at the YD-PB transition. During the Holocene, the 3,5Bd/V ratio decreased again and reached the lowest values near the top of the core.

The 3,5Bd/V ratios in the core from the Okhotsk Sea range from 0.10 to 0.23 (Fig. 3, IId) (standard deviation: 0.02). The values were rather uniform throughout the record, with the exception of a maximum during the PB, and the ratio remained rather stable afterwards.

The $(Ad/Al)_s$ and $(Ad/Al)_v$ ratios ranged from 0.19 to 0.80 (standard deviation: 0.24) and 0.51 to 1.04 (standard deviation: 0.26), respectively, in the Bering Sea (Fig. 3, Ie, f). Maxima in $(Ad/Al)_s$ and $(Ad/Al)_v$ were reached in the Holocene and YD. The Ad/Al ratio in the Bering Sea showed low values during the PB and increased towards the early Holocene, when highest values of Ad/Al were obtained.

In the Okhotsk Sea, the $(Ad/Al)_s$ and $(Ad/Al)_v$ ratios are overall similar and range from 0.30 to 0.79 (standard deviation: 0.24) and from 0.22 to 0.89 (standard deviation: 0.26), respectively (Fig 3, IIe, f). The $(Ad/Al)_v$ ratio decreased slowly until

10.5 ka BP when the biomarker MARs reached maxima. All minima and maxima in both indices occurred in the PB. Throughout the rest of the Holocene, Ad/Al values remained rather constant.

4.3. Sea surface temperature in the Bering Sea (TEX^L_{86})

The SST estimates derived from the TEX^L_{86} index are shown in Fig. 4, Ic. The deglacial evolution of the TEX^L_{86}-derived SST ranging from 4.48 to 10.81 °C. The SST in the Bering Sea remained rather constant during the LGM and the ED. The onset of the B/A is characterized by an abrupt temperature increase of ~2 °C, followed by a decrease at the end of the B/A. At the end of the YD, the SST abruptly increased by ~2 °C, while staying rather constant from 11.5 ka BP to 10 ka BP. At the end of PB, the SST progressively dropped by ~1 °C. During the Holocene, the SST ranged between 8.0 °C and 9.7 °C.

5. Discussion

5.1. Vegetation changes in the two river basins

5.1.1. Yukon River Basin

As the climate warmed during the transition from the LGM to the ED, moisture increased and an increasing number of thermokarst lakes developed in Alaska, especially after about 16–14 ka BP (Bigelow, 2013; Walter et al., 2007). We observe a increase in S/V ratios from the ED to the B/A, indicating increasing contributions of angiosperms around this time, extending into the B/A (Fig. 3, Ia). The S/V and C/V ratios are also influenced by degradation of lignin, with increasing ratios suggesting a lower degradation state (Hedges et al., 1988), but there is no parallel decrease in the more commonly used degradation indicator, i.e., the Ad/Al ratios, at the same time (Fig. 3, Ie, f). Anderson et al. (2003) also found birch pollen becoming significantly more prevalent after about 16 ka BP from western Alaska to the Mackenzie River. Coevally, the Paq index (Fig. 3, Ic, from Meyer et al., 2019) shows an increase, indicating wetland expansion.

There is evidence that herb-dominated tundra was replaced by *Betula-Salix* shrub tundra around Trout Lake (the northern Yukon) during the B/A (Fritz et al., 2012) as the climate warmed and became more humid than during the ED. In line with these observations, our C/V ratios indicate that the contribution of non-woody plant tissues was lower in the B/A than in the ED (Fig. 3, Ib).

https://doi.org/10.5194/cp-2022-67
Preprint. Discussion started: 6 September 2022

After the B/A, the summer temperatures during the YD dropped by ~1.5 °C (Fritz et al., 2012), thus cold-adapted non-arboreal plants briefly increased in abundance (Fritz et al., 2012). The S/V ratios indicate that the non-woody angiosperm plants' contribution reached a maximum in the Yukon Basin during the YD-PB transition (Fig. 3, Ia). Since the opening of the Bering Strait (~11 ka BP, Jakobsson et al., 2017), a trend of increase in *Betula* was observed in eastern Beringia (Fritz et al., 2012; Kaufman et al., 2015) which indicates a progressively more maritime climate developing in response to changes in the marine environment (Igarashi and Zharov, 2011). Since vegetation responds to changes in both temperature and moisture, significant *Populus/Salix* woodland development occurred in interior Alaska and in the Yukon Territory during the early Holocene (Anderson et al., 2003). However, the expansion of these angiosperm plants is not reflected in our S/V record (Fig. 3, Ia), the interpretation of S/V ratios may be complicated by the influence of degradation processes during the early Holocene. Pollen assemblages from northern Siberian soils have shown that woody plants occurred only after the onset of the Holocene (Binney et al., 2009), which agrees with a decrease in the C/V ratios since the early PB into the early Holocene (Fig. 3, Ib).

We compare our S/V and C/V ratios with published values from sediment cores, surface sediments and suspended materials in the Arctic and subarctic (Fig. 5). Such plots can help to identify the main types of plant tissues the lignin phenols are derived from, and enable the detection of potential degradation effects.

The S/V and C/V ratios from our Bering Sea core compare favorably with those from a core recovered from the Chukchi shelf covering parts of the B/A and the YD as well as the late Holocene (Martens et al., 2019) (Fig. 5). This may suggest that a similar type of vegetation prevailed across much of Beringia. After the opening of the Bering Strait, Pacific waters flowed into the Chukchi Sea, and it is conceivable that the terrestrial material transported to the Bering Sea by the Yukon River may have been in part be transported into the Chukchi Sea. The top of our core dates to the early Holocene, a period that was characterized by more wide-spread broad-leaf angiosperm vegetation than today, which might explain the offset between our early Holocene S/V and C/V ratios and those reported for Yukon River surface sediment (S/V: 0.28, C/V: 0.14) (Feng et al., 2015) and dissolved organic carbon in the Yukon (S/V: 0.47, C/V: 0.14) (Amon et al., 2012) at present. Degradation of lignin in sediments may explain some of the discrepancy between sediment data and S/V and

https://doi.org/10.5194/cp-2022-67
Preprint. Discussion started: 6 September 2022

C/V ratios reported from suspended materials collected in the modern Lena River (Fig. 5). As the Amur River catchment is dominated by gymnosperms at present (Seki et al. 2014), the S/V ratios of the Amur River and Okhotsk Sea surface sediments (Seki et al., 2014) are lower than in the Bering Sea core (Fig. 5).

The highest values of the 3,5Bd/V ratio correlate with the enhanced degradation of lignin phenols around 17.5 ka BP (Fig. 3, Id). This suggests that degraded OM is the dominant source for the lignin phenols at this time, in agreement with previous studies (Meyer et al., 2016, 2019). Global melt water pulses according to Lambeck et al. (2014) occurred during the following time periods: MWP-1A from 14.6 to 14.0 ka BP and the MWP-1B from 11.5 to 10.5 ka BP. The 3,5Bd/V and $(Ad/Al)_s$ ratios decreased slowly from the ED to the MWP-1A, which indicates that the change 3,5Bd/V values from the LGM to the early B/A reflects a variable degree of OM degradation, rather than expansion of wetlands or peatlands. The 3,5Bd/V also featured a short maximum during the late YD and early PB when the 3,5Bd/V signal is likely dominantly ascribed to increases in wetland or peatland sources, as there is no parallel maximum in Ad/Al ratios (Fig. 3, Id, e, f).

This pattern of 3,5 Bd/V change is not in agreement with the Paq ratio determined for the same core earlier (Meyer et al., 2019), although both proxies may reflect wetland expansion (Goñi et al., 2000b; Amon et al., 2012). The temporal evolution of Paq is similar to that of S/V and C/V, where Paq began to increase in the ED and reached its maximum in the YD-PB transition (Fig. 3, Ic), indicating that the proxies are influenced to some extent by degradation.

Notably, a lower degree of OM degradation is indicated for periods with high MAR of terrigenous OM, indicating that rapid transport and burial might contribute to better preservation of lignin. This better preservation, in particular during the early PB (Fig. 3e, f), is in agreement with previous studies (Anderson et al., 2003; Meyer et al., 2019). Kuehn et al. (2014) found that increases in biological export production and remineralization of OM in the Bering Sea during the B/A and PB, reduced oxygen concentration to below 0.1 ml L^{-1} and caused the occurrence of laminated sediments (Fig. 2c). This anoxic condition in the Bering Sea during the B/A and PB also slowed down rates of OM decomposition and increased the accumulation of OM.

With progressive sea-level rise through the early Holocene, the distance between the Yukon River mouth and the core-site increased, leading to longer transport distance and stronger degradation of lignin. In the East Siberian Arctic Shelf, Tesi et

https://doi.org/10.5194/cp-2022-67
Preprint. Discussion started: 6 September 2022

al. (2014) found that lignin concentrations exhibit a marked decrease by three orders of magnitude with increasing distance from the coast.

In summary, our data together with published evidence indicate that in the Yukon Basin, vegetation change and wetland expansion began in the ED. Angiosperm plant contribution and wetland extent all reached their maxima during the PB, both decreasing and stabilizing at lower levels after the PB. During the PB, terrigenous OM appeared least degraded, suggesting rapid supply and burial of rather well-preserved terrigenous OM.

5.1.2. Amur River Basin

The lowest contribution of non-woody angiosperms as indicated by low S/V and C/V ratios occurred at 16.6 ka BP (Fig. 3, IIa, b). Subsequently, both ratios increased and reached maxima during the PB, suggesting expansion of angiosperms and non-woody tissues contributing substantially to lignin. After the PB, the S/V decreased rapidly and remained stable during the Holocene, while the C/V ratio showed a second maximum at 9.2 ka BP suggesting an increasing contribution of non-woody angiosperms in the PB (Fig. 3, IIa, b). In agreement with our data, published lipid records provide evidence that the vegetation in the Amur Basin did not change significantly in the ED (Seki et al., 2012). Winterfeld et al. (2018) found a general synchronicity of Amur River discharge and northward extent of monsoon precipitation in the early Holocene. Climate warming associated with high moisture supply allowed the expansion of birch-alder forests in the Amur Basin in the PB (Bazarova et al., 2008; Igarashi and Zharov, 2011).

C/V and S/V ratios indicate that the contribution of non-woody gymnosperm tissue was higher in the early than in the later deglaciation (Fig. 6), similar to what has been reported from East Siberian Shelf records (Keskitalo et a., 2017). Apparently, the YD caused only minor vegetation changes in the East Asian hinterland (Igarashi and Zharov, 2011). Our lignin records for this period are in agreement with previous studies that indicated that the Lower Amur River basin mainly featured shrub birch-alder forests and rare *Pinus* (Bazarova et al., 2008; Seki et al., 2012).

Non-woody angiosperm plant contributions to the Okhotsk Sea sediment strongly increased during the PB (Fig. 3, IIa, b), when the summer insolation and regional temperatures reached the highest values since the LGM. Significant vegetation changes in the Amur Basin thus started in the PB period, temporally offset from the Yukon Basin, and the contribution of angiosperms from 14.6 ka BP to 9 ka

BP appears to be higher than during the ED (Fig. 6). Bazarova et al. (2008) reported based on pollen analyses that a turning point in vegetation development in the Amur Basin occurred at a boundary of 10 ka BP. The Middle Amur depression registered the first appearance of broad-leaved species pollen and a prevalence of spores over arboreal pollen at that time (Bazarova et al., 2008). The C/V ratio did not decrease as rapidly as the S/V ratio after the peak and showed a second maximum at ~9 ka BP. Some pollen of *Picea* (such as *P.* glauca and *P.* mariana) yield exceptionally high amounts of cinnamyl phenols (Hu et al., 1999), which may have affected the C/V ratio as the end member of woody/non-woody tissues. An et al. (2000) concluded that lakes were deepest and most extensive around 10 ka BP in northeastern China (the upper Amur basin), and 3,5Bd/V and Paq values reached maxima at the same time (Fig. 3, IId, c) suggesting wetland extent peaked during the PB. Therefore, wetland plants which have broad leaves, such as sedges, may also have a positive influence on the C/V ratio.

The S/V and C/V data from the Holocene part of our core do not agree with published values for the Okhotsk Sea and Amur River surface sediments (Fig. 6). During the past 250 years, vegetation was marked by significant rises of gymnosperms, such as pines, combined with the reduction in the swamp area and a large increase in fire activity (Seki et al., 2014), likely resulting in higher contributions of gymnosperm to the surface sediment while these changes are not resolved in the samples analysed for our record.

The 3,5Bd/V and Paq ratios of the Okhotsk Sea both display relatively high values during the PB (Fig. 3, IId, c). Seki et al. (2012) found high Paq values during the PB in a nearby sediment core XP07-C9, and the values in their core were higher than in ours (Fig. 3, IIc). Spores of Sphagnum show a distinct peak during the PB (Morley et al., 1991), reflecting an expansion of mesic and boggy habitats. Our records together with published evidence thus suggest that permafrost destabilization and wetland expansion in the Amur Basin occurred only at the beginning of the PB, while those processes were initiated much earlier in the Yukon basin.

The Ad/Al values were decreasing until 10.5 ka BP and reached minima during the PB (Fig. 3e, f), indicating that low temperatures on land on the one hand, and rapid burial in marine sediments during shelf flooding and coastal erosion during MWP-1B on the other hand, contributed to the Ad/Al signals. In the course of climate amelioration from around 11.6 ka BP (Tarasov et al, 2009), the rates of vegetation

https://doi.org/10.5194/cp-2022-67
Preprint. Discussion started: 6 September 2022

development, wetland expansion and Amur River discharge (Fig. 2f) all displayed maxima in the PB. Generally higher Ad/Al values in the later part of the PB suggest that fluvial runoff supplied more degraded lignin. Aerobic degradation of OM in soils by fungi has also been shown to increase Ad/Al values (Goñi et al., 1993). Reports that the degradation degree of Lena River-derived OM and surface sediments of Buor Khaya Bay are similar (Winterfeld et al., 2015), suggest that the oxidative degradation occurred mainly on land. The Okhotsk Sea shelf is narrower than the Bering Shelf and Siberian shelves, the lateral shelf transport times (i.e., the cumulative time a particle spends in sedimentation-resuspension cycles) of the Okhotsk shelf are therefore likely to be much shorter than what has been reported for the Laptev Shelf (Bröder et al., 2018), further supporting our interpretation.

In summary, our records indicate that in the Amur Basin vegetation change and wetland expansion began during the PB and in the early Holocene, in agreement with previous paleo-vegetation studies. This timing is different from observed changes in the Yukon Basin. However, similar to the Yukon Basin, the wetland extent and non-woody angiosperm contribution were reduced and stabilized after the PB in the Amur Basin. The increased vegetation and wetland indices, as well as increased degradation of lignin in the Okhotsk Sea sediment at the end of the PB, may be related to changes in the source of OM (shelf and coastal erosion vs river transported material).

5.2. Terrigenous OM mobilization during the deglaciation

Permafrost remobilization has a strong impact on local topography, vegetation, and OM fate (Feng et al., 2013; Walter Anthony et al., 2014). We observed distinct MAR peaks of terrigenous biomarkers in both sediment cores, but the temporal evolution of MARs and the relative magnitude of change differ between the sites.

In the Bering Sea, lignin MAR began to increase at 17.5 ka BP (Fig. 2c), but evidence for change in vegetation in the Yukon Basin was only found near 15 ka BP and the Yukon River discharge did not increase until 16.5 ka BP (Wang et al., 2021). Therefore, the increased lignin MAR may correspond to the mobilization of terrestrial OM from surface sources, like permafrost soils. Previous studies indicated that Ice Complex Deposit (ICD) samples yield relatively high S/V and C/V ratios, indicating the OM likely to stem from grass-like material typical of tundra or steppe biome (Schirrmeister et al., 2013; Tesi et al., 2014; Winterfeld et al., 2015). Thus, the increased S/V, C/V, and Paq values near 17.5 ka BP (Fig. 3, Ia–c) lend support to the

https://doi.org/10.5194/cp-2022-67
Preprint. Discussion started: 6 September 2022

notion that permafrost of the Yukon Basin may have begun to be remobilized in the ED.

Vaks et al. (2020) found that Siberian permafrost is vulnerable to warming when Arctic sea-ice is absent. Retreat of sea ice will increase the SST, and open waters increase the moisture content of the atmosphere, so the transport of heat from the ocean via atmospheric pathways to continental interiors increases (Ballantyne et al., 2013; Vaks et al., 2020). Praetorius et al. (2015) found that SST warming commenced around 16.5 ka BP (core 85JC, Fig. 4, If) in the northern Gulf of Alaska, and Méheust et al. (2018) observed rising SST of the northeast Pacific by ~1.5 °C near 16 ka BP (core SO202-27-6, Fig. 4, Ie) which agrees with our SST record (core SO202-18-3/6, Fig. 4, Ic). The same authors reconstructed sea-ice extent based on the IP_{25} proxy to decrease from around 16 ka BP in the Northeast Pacific (Fig. 4, Ie). Jones et al. (2020) reported that the sea ice in the Bering Sea is highly sensitive to small changes in winter insolation and atmospheric CO_2. Further evidence for regional climate warming in the hinterland of Alaska is provided by the Brooks Range glacial melting during a time of widespread cooling on the Northern Hemisphere (Dyke, 2004; Wang et al., 2021). The permafrost of the Yukon Basin may thus have begun to be remobilized at ~16 ka BP. Examining the records in more detail reveals that the lipid MAR increase lags behind lignin MAR in the ED, lipid MAR increase at a similar time to when the rate of sea-level change began to increase (Fig. 2c). This suggests that lipid flux can reflect permafrost mobilization via coastal erosion (Meyer et al., 2019).

In the B/A, all biomarker fluxes increased and reached short maxima (Fig. 2c, d). Warming may have caused widespread permafrost thaw in the Yukon Basin. At this time, SST increased, sea-ice cover decreased (Méheust et al., 2018), and an increase in river discharge was reconstructed (Wang et al., 2021), which may have fostered diatom bloom events.

Little degraded lignin may also have been derived from ice-rich ICD deposits rapidly eroding during warming phases and sea-level rise induced mobilization of permafrost deposits. The degree of lignin degradation was lower than before, and combined with S/V and C/V ratios (Fig. 5), we suggest that the OM deposited in the Bering Sea during the B/A may have been derived from ICD OM. Similar to our findings, Martens et al. (2019) found relatively high lignin fluxes in the Chukchi Sea during the B/A (Fig. 2e) and showed that lignin deposited during this period was

https://doi.org/10.5194/cp-2022-67
Preprint. Discussion started: 6 September 2022

poorly degraded. The authors interpreted this degradation state as permafrost OM from ICD being the dominant source. The relative contribution of ICD and the main pathway of transportation (abrupt thaw or gradual thaw on land) cannot be deduced from our data alone. Further analyses may reveal possible ICD contributions to lignin exported to the marine realm during this interval.

During the YD-PB transition, the Northern Hemisphere experienced an abrupt temperature increase, the maxima of biomarker MAR (Fig. 2c) and wetland indices (Fig. 3I) indicate that the permafrost remobilization in the Yukon Basin reached a peak at this time. The Yukon River discharge increased during the PB (Wang et al., 2021) which can also promote lignin flux. Evidence for widespread permafrost decomposition and wetland expansion at the same time has been reported from the Bering Sea (Meyer et al., 2019), the Siberian-Arctic (Tesi et al., 2016; Martens et al., 2020), and eastern Beringia (Kaufman et al., 2015). Bering Sea sediments deposited during the time intervals of lignin MAR peaks were laminated (Fig. 2c), indicating increased export productivity and terrigenous OM supply may have promoted anoxic conditions during the YD-PB transition.

Different from the Bering Sea records, lignin MAR did not yet increase in the Okhotsk Sea during the ED (Fig. 2d), except for a short peak at the transition from the ED to the B/A. SSTs were higher in the Northeast Pacific and the Bering Sea than in the Northwest Pacific and Okhotsk Sea during the ED, and the IP_{25} value was relatively high in the Okhotsk Sea (Fig. 4, IIc), indicating the sea ice of the Okhotsk Sea did not begin to retreat in the ED (Lo et al., 2018). Caissie et al. (2010) found that the first detectable concentration of alkenones in the Bering Sea sediment at 16.7 ka BP occurred earlier than in the Okhotsk Sea, although the Bering Sea is located further north than the Okhotsk Sea. In addition, the discharge of the Amur River began to increase at ~16 ka BP, and the vegetation of the Amur Basin had not begun to change during the ED. As a consequence, the permafrost of the Amur Basin may have not yet been remobilized in the ED (Vaks et al., 2013, 2020; Winterfeld et al., 2018; Meyer et al., 2019).

Biomarker MARs increased and lignin degradation decreased slightly during the B/A warm interval. The rate of sea-level change reached a peak during MWP-1A (Fig. 2d) which likely also caused an increase in the rate of coastal erosion. Thus, the increased biomarker MAR during the B/A may be attributed largely to coastal erosion, and high rates of sedimentation promoted burial and reduced degradation of OM.

https://doi.org/10.5194/cp-2022-67
Preprint. Discussion started: 6 September 2022

Therefore, this suggests that both types of biomarkers are supplied via the same erosive process, in contrast to findings from the modern-day Arctic.

From the YD to the PB, the Northern Hemisphere experienced an abrupt temperature increase and the SST of the North Pacific increased significantly (Max et al., 2012; Riethdorf et al., 2013; Méheust et al., 2016, 2018; Meyer et al., 2016, 2017). All biomarker MARs in the Okhotsk Sea increased and reached maxima in the YD-PB transition. The permafrost of the Amur Basin may have begun to be remobilized coevally with previously reported periods of stalagmite growth starting after the PB in the south of Siberia, which indicates the decay of permafrost and opening of water conduits into the caves (Vaks et al. 2013, 2020). A pronounced lignin flux maximum occurred during MWP-1B, coinciding with a period of enhanced discharge from the Amur River. This implies that hinterland permafrost thawing played a more important role in the land-ocean OM transport during the later deglaciation. The Ad/Al ratios decreased when the biomarker MAR peaked in the MWP-1B which may correspond to better preservation during rapid burial, or higher contribution of ICD OM and fresh angiosperm debris. Conversely, Martens et al. (2019) found that the degradation degree of lignin in the Chukchi Sea sediment increased during rapid sea-level rise between 13 and 11 ka BP, which might be attributed to ongoing degradation during transport to the core site during times of increasing distance from the shoreline.

MARs decrease drastically after maxima in both the Okhotsk and Bering Seas (Fig. 2c, d). The Amur Basin was completely covered with permafrost during the LGM and almost all of the permafrost was lost as a result of permafrost mobilization (Vaks et al., 2013; Vandenberghe et al., 2014). Thus, the contribution of permafrost OM from the Amur Basin to the marine sediment began to decrease in the early Holocene in agreement with the results of Seki et al. (2012).

In summary, the permafrost of the Amur Basin began to be remobilized in the PB later than in the Yukon Basin. We suggest that this is caused by decreased sea ice or increased SST in the Bering Sea during the ED, while the Okhotsk Sea remained ice-covered.

Conclusions:

By analyzing mass accumulation rates of terrigenous biomarkers in sediments from the Bering and Okhotsk Seas, we provide the first downcore records of lignin from the Yukon and Amur Basins covering the early deglaciation to the Holocene. We find that vegetation changed earlier in the Yukon than in the Amur Basin. Although S/V, C/V and 3,5Bd/V ratios can reflect vegetation change and wetland development, the degradation state of lignin strongly overprints these proxy signals and should be considered as a function of temperature, transport distance and burial rate. Similar to changes in vegetation, we observe that degradation and remobilization of permafrost of the Yukon Basin also occurred earlier than in the Amur Basin. Sea-ice extent and SSTs of adjacent ocean areas might have had a strong influence on the timing of hinterland permafrost mobilization. Our study reveals that lignin transported by surface runoff may account for significant proportions of lignin during inland warming, but export of lignin and lipids do not always occur via different pathways, as both biomarker groups can be contributed from rapidly eroding deep deposits during phases of rapid permafrost thaw. In contrast to modern day evidence suggesting different pathways for lipid and lignin biomarker transport, our records imply that during glacial peaks of permafrost decomposition, lipids and lignin might have been delivered to the ocean by identical processes, i.e., runoff and erosion.

Authors' contributions

MC measured and compiled lignin data, and wrote the manuscript with the help of all co-authors. JH was responsible for all biomarker analyses. LLJ and RT provided samples. VM carried out sea surface temperature measurements of SO202-18-3/6. GM designed the study. All authors participated in the discussion of results and conclusions and contributed to the final version of the paper.

Competing interests

The authors declare that they have no conflict of interest.

Acknowledgements

We thank the masters and crews of R/V Sonne for their professional support during cruises SO202 (INOPEX) and SO178 (KOMEX). Hartmut Kuehn is acknowledged for providing total organic carbon and dry bulk density data of site SO202-18-3/6. Mengli Cao thanks the China Scholarship Council (CSC) and POLMAR- Helmholtz Graduate School for Polar and Marine Research for additional support. We are also grateful to laboratory and computer staff at Alfred Wegener Institute. The biomarker data generated in this study are accessible at the database Pangaea: ...

References

Amon, R. M. W., Rinehart, A. J., Duan, S., Louchouarn, P., Prokushkin, A., Guggenberger, G., Bauch, D., Stedmon, C., Raymond, P.A., Holmes, R. M., McClelland, J. W., Peterson, B. J.,

Walker, S. A., and Zhulidov, A. V.: Dissolved organic matter sources in large Arctic rivers, Geochim. Cosmochim. Ac., 94, 217–237, http://dx.doi.org/10.1016/j.gca.2012.07.015, 2012.
An, Z., Porter, S. C., Kutzbach, J. E., Wu, X., Wang, S., Liu, X., Li, X., and Zhou, W.: Asynchronous Holocene optimum of the east Asian monsoon, Quaternary Sci. Rev., 19, 743–762, https://doi.org/10.1016/S0277-3791(99)00031-1, 2000.
Anderson, P. M., Edwards, M. E., and Brubaker, L. B.: Results and paleoclimate implications of 35 years of paleoeco logical research in Alaska, in: The Quaternary Period in the United States, edited by: Gillespie, A. R., Porter, S. C., and Atwater, B. F., Elsevier, Amsterdam, 427–440, https://doi.org/10.1016/S1571-0866(03)01019-4, 2003.
Ballantyne, A. P., Axford, Y., Miller, G. H., Otto-Bliesner, B. L., Rosenbloom, N., and White, J. W. C.: The amplification of Arctic terrestrial surface temperatures by reduced sea-ice extent during the Pliocene, Palaeogeogr. Palaeocl., 386, 59–67, http://dx.doi.org/10.1016/j.palaeo.2013.05.002, 2013.
Bazarova, V. B., Klimin, M. A., Mokhova, L. M., and Orlova, L. A.: New pollen records of Late Pleistocene and Holocene changes of environment and climate in the Lower Amur River basin, NE Eurasia, Quatern. Int., 179, 9–19, https://doi.org/10.1016/j.quaint.2007.08.015, 2008.
Bigelow, N. H.: Pollen Records, Late Pleistocene | Northern North America, in: Encyclopedia of Quaternary Science (second Edition), edited by: Elias, S. A., Mock, C. J., Elsevier, 39–51, https://doi.org/10.1016/B978-0-444-53643-3.00187-4, 2013.
Binney, H. A., Willis, K. J. Edwards, M. E., Bhagwat, S. A., Anderson, P. M., Andreev, A. A., Blaauw, M., Damblon, F., Haesaerts, P., Kienast, F., Kremenetski, K. V., Krivonogov, S. K., Lozhkin, A. V., Macdonald, G. M., Novenko, E. Y., Oksanen, P., Sapelko, T. V., Väliranta, M., and Vazhenina, L.: The distribution of late-Quaternary woody taxa in northern Eurasia: evidence from a new macrofossil database, Quaternary Sci. Rev., 28, 2445–2464, https://doi.org/10.1016/j.quascirev.2009.04.016, 2009.
Brown, J., Ferrians, O., Heginbottom, J. A., and Melnikov, E.: Circum-Arctic Map of Permafrost and Ground-Ice Conditions, version 2, Boulder, Colorado USA, NSIDC: National Snow and Ice Data Center [data set], https://doi.org/10.7265/skbg-kf16, 2002.
Bröder, L., Tesi, T., Andersson, A., Semiletov, I., and Gustafsson, Ö.: Bounding cross-shelf transport time and degradation in Siberian-Arctic land-ocean carbon transfer, Nat. Commun., 9, 806, https://doi.org/10.1038/s41467-018-03192-1, 2018.
Caissie, B. E., Brigham-Grette, J., Lawrence, K. T., Herbert, T. D., and Cook, M. S.: Last Glacial Maximum to Holocene sea surface conditions at Umnak Plateau, Bering Sea, as inferred from diatom, alkenone, and stable isotope records, Paleoceanography, 25, PA1206, https://doi.org/10.1029/2008PA001671, 2010.
Couture, N. J., Irragang, A., Pollard, W., Lantuit, H., and Fritzs, M.: Coastal erosion of permafrost soils along the Yukon Coastal Plain and fluxes of organic carbon to the Canadian Beaufort Sea, J. Geophys. Res.-Biogeo., 123, 406–422, https://doi.org/10.1002/2017JG004166, 2018.
Dullo, W. C., Biebow, N., and Georgeleit, K.: SO178-KOMEX Cruise Report: Mass Exchange Processes and Balances in the Okhotsk Sea, GEOMAR Report, Germany, 110 pp., 2004.
Dyke, A. S.: An outline of North American deglaciation with emphasis on central and northern Canada, in: Developments in Quaternary Sciences, edited by: Ehlers, J., Gibbard, P. L., Elsevier, volume 2, part B, 373–424, https://doi.org/10.1016/S1571-0866(04)80209-4, 2004.
Eglinton, G. and Hamilton, R. J.: Leaf epicuticular waxes: The waxy outer surfaces of most plants display a wide diversity of fine structure and chemical constituents, Science, 156, 1322–1335, https://doi/10.1126/science.156.3780.1322, 1967.
Erdtman, H.: Lignins: Occurrence, Formation, Structure and Reactions, in: Journal of Polymer Science Part B: Polymer Letters, sdited by: Sarkanen, K. V., Ludwig, C. H., John Wiley & Sons, Inc., New York, 916 pp, 1971.
Feng, X., Vonk, J. E., van Dongend, B. E., Gustafssone, Ö., Semiletov, I. P., Dudarev, O. V., Wang, Z., Montlucon, D. B., Wacker, L., and Eglinton, T. I.: Differential mobilization of terrestrial carbon pools in Eurasian Arctic river basins, P. Natl. Acad. Sci. USA, 110, 14168–14173, https://doi.org/10.1073/pnas.1307031110, 2013.
Feng, X., Gustafssone, Ö., Holmes, R.M., Vonk, J. E., van Dongend, B. E., Semiletov, I. P., Dudarev, O. V., Yunker, M. B., Macdonald, R. W., Montlucon, D. B., and Eglinton, T. I.:

https://doi.org/10.5194/cp-2022-67
Preprint. Discussion started: 6 September 2022

Multi-molecular tracers of terrestrial carbon transfer across the pan-Arctic: comparison of hydrolyzable components with plant wax lipids and lignin phenols, Biogeosciences, 12, 4841–4860, https://doi.org/10.5194/bg-12-4841-2015, 2015.

Ficken, K. J., Li, B., Swain, D. L., and Eglinton, G.: An *n*-alkane proxy for the sedimentary input of submerged/floating freshwater aquatic macrophytes, Org. Geochem., 31, 745–749. https://doi.org/10.1016/S0146-6380(00)00081-4, 2000.

Fritz, M., Herzschuh, U., Wetterich, S., Lantuit, H., De Pascale, G. P., Pollard, W. H., and Schirrmeister, L.: Late glacial and Holocene sedimentation, vegetation, and climate history from easternmost Beringia (northern Yukon Territory, Canada), Quaternary Res., 78, 549–560, http://dx.doi.org/10.1016/j.yqres.2012.07.007, 2012.

Gersonde, R.: The expedition of the research vessel "Sonne" to the subpolar North Pacific and the Bering Sea in 2009 (SO202-INOPEX), Berichte zur Polar- und Meeresforschung/ Reports on polar and marine research, Bremerhaven, Alfred Wegener Institute for Polar and Marine Research, 643, 323 pp, 2012.

Goñi, M. A., Nelson, B., Blanchette, R. A., and Hedges, J. I.: Fungal degradation of wood lignins: geochemical perspectives from CuO-derived phenolic dimers and monomers, Geochim. Cosmochim. Ac., 57, 3985–4002, https://doi.org/10.1016/0016-7037(93)90348-Z, 1993.

Goñi, M. A. and Montgomery, S.: Alkaline CuO Oxidation with a Microwave Digestion System: Lignin Analyses of Geochemical Samples, Anal. Chem., 72, 3116–3121, https://doi.org/10.1021/ac991316w, 2000a.

Goñi, M. A., Yunker, M. B., Macdonald, R. W., Eglinton, T. I.: Distribution and sources of organic biomarkers in arctic sediments from the Mackenzie River and Beaufort Shelf, Mar. Chem., 71, 23–51, https://doi.org/10.1016/S0304-4203(00)00037-2, 2000b.

Hedges, J. I. and Mann, D. C.: The characterization of plant tissues by their lignin oxidation products, Geochim. Cosmochim. Acta 43, 1803-1807, https://doi.org/10.1016/0016-7037(79)90028-0, 1979.

Hedges, J. I., Blanchette, R. A., Weliky, K., and Devol, A. H.: Effects of fungal degradation on the CuO oxidation products of lignin: A controlled laboratory study, Geochim. Cosmochim. Ac., 52, 2717–2726, https://doi.org/10.1016/0016-7037(88)90040-3, 1988.

Holmes, R. M., McClelland, J. W., Peterson, B. J., Tank, S. E., Bulygina, E., Eglinton, T. I., Gordeev, V. V., Gurtovaya, T. Y., Raymond, P. A., Repeta, D. J., Staples, R., Striegl, R. G., Zhulidov, A. V., and Zimov, S. A.: Seasonal and Annual Fluxes of Nutrients and Organic Matter from Large Rivers to the Arctic Ocean and Surrounding Seas, Estuar. Coasts, 35, 369–382, https://doi.org/10.1007/s12237-011-9386-6, 2012.

Hu, F. S., Hedges, J. I., Gordon, E. S., and Brubaker, L. B.: Lignin biomarkers and pollen in postglacial sediments of an Alaskan lake, Geochim. Cosmochim. Ac., 63, 1421–1430, https://doi.org/10.1016/S0016-7037(99)00100-3, 1999.

Hugelius, G., Strauss, J., Zubrzycki, S., Harden, J. W., Schuur, E. A. G., Ping, C.-L., Schirrmeister, L., Grosse, G., Michaelson, G. J., Koven, C. D., O'Donnell, J. A., Elberling, B., Mishra, U., Camill, P., Yu, Z., Palmtag, J., and Kuhry, P.: Estimated stocks of circumpolar permafrost carbon with quantified uncertainty ranges and identified data gaps, Biogeosciences, 11, 6573–6593, https://doi.org/10.5194/bg-11-6573-2014, 2014.

Igarashi, Y. and Zharov, A. E.: Climate and vegetation change during the late Pleistocene and early Holocene in Sakhalin and Hokkaido, northeast Asia, Quaternary Int., 237, 24–31, https://doi.org/10.1016/j.quaint.2011.01.005, 2011.

Jakobsson, M., Pearce, C., Cronin, T. M., Backman, J., Anderson, L. G., Barrientos, N., Björk, G., Coxall, H., de Boer, A., Mayer, L. A., Mörth, C.-M., Nilsson, J., Rattray, J. E., Stranne, C., Semiletov, I., and O'Regan, M.: Post-glacial flooding of the Bering land bridge dated to 11 cal ka BP based on new geophysical and sediment records, Clim. Past, 13, 991–1005, https://doi.org/10.5194/cp-13-991-2017, 2017.

Jones, M. C., Berkelhammer, M., Keller, K. J., Yoshimura, K., and Wooller, M. J.: High sensitivity of Bering Sea winter sea ice to winter insolation and carbon dioxide over the last 5500 years, Science Advances, 6, eaaz9588, 2020.

Kaufman, D. S., Axford, Y. L., Henderson, A. C. G., Mckay, N. P., Oswald, W. W., Saenger, C., Anderson, R. S., Bailey, H. L., Clegg, B., Gajewshi, K., Hu, F. S., Jones, M. C., Massa, C., Routson, C. C., Werner, A., Wooller, M. J., and Yu, Z.: Holocene climate changes in eastern

https://doi.org/10.5194/cp-2022-67
Preprint. Discussion started: 6 September 2022

Beringia (NW North America)-A systematic review of multi-proxy evidence, Quaternary Sci. Rev., 312–339, https://doi.org/10.1016/j.quascirev.2015.10.021, 2015.

Kennedy, K. E., Froese, D. G., Zazula, G. D., Lauriol, B.: Last glacial maximum age for the northwest Laurentide maximum from the eagle river spillway and delta complex, northern Yukon, Quat. Sci. Rev. 29, 1288–300, https://doi.org/10.1016/j.quascirev.2010.02.015, 2010.

Keskitalo, K., Tesi, T., Bröder, L., Andersson, A., Pearce, C., Sköld, M., Semiletov, I. P., Dudarev, O. V., and Gustafsson, Ö.: Sources and characteristics of terrestrial carbon in Holocene-scale sediments of the East Siberian Sea, Clim. Past, 13, 1213–1226, https://doi.org/10.5194/cp-13-1213-2017, 2017.

Kim, J.-H., van der Meer, J., Schouten, S., Helmke, P., Willmott, V., Sangiorgi, F., Koç, N., Hopmans, E. C., and Sinninghé Damsté J. S.: New indices and calibrations derived from the distribution of crenarchaeal isoprenoid tetraether lipids: Implications for past sea surface temperature reconstructions, Geochim. Cosmochim. Ac., 74, 4639–4654, https://doi.org/10.1016/j.gca.2010.05.027, 2010.

Köhler, P., Knorr, G., and Bard, E.: Permafrost thawing as a possible source of abrupt carbon release at the onset of the Bölling/Allerod, Nat. Commun., 5, 5520, http://doi.org/10.1038/ncomms6520, 2014.

Kuehn, H., Lembke-Jene, L., Gersonde, R., Esper, O., Lamy, F., Arz, H., Kuhn, G., and Tiedemann, R.: Laminated sediments in the Bering Sea reveal atmospheric teleconnections to Greenland climate on millennial to decadal timescales during the last deglaciation, Clim. Past, 10, 2215–2236, https://doi.org/10.5194/cp-10-2215-2014, 2014.

Lambeck, K., Rouby, H., Purcell, A., Sun, Y., and Sambridge, M.: Sea level and global ice volumes from the Last Glacial Maximum to the Holocene, P. Natl. Acad. Sci. USA, 11, 15296–15303, https://doi.org/10.1073/pnas.1411762111, 2014.

Lantuit, H., Overduin, P.P., Couture, N., Wetterich, S., Aré, F., Atkinson, D., Brown, J., Cherkashov, G., Drozdov, D., Forbes, D.L., Graves-Gaylord, A., Grigoriev, M., Hubberten, H.-W., Jordan, J., Jorgenson, T., Ødegård, R. S., Ogorodov, S., Pollard, W. H., Rachold, V., Sedenko, S., Solomon, S., Steenhuisen, F., Streletskaya, I., and Vasiliev, A.: The Arctic Coastal Dynamics Database: A New Classification Scheme and Statistics on Arctic Permafrost Coastlines, Estuar. Coasts, 35, 383–400, https://doi.org/10.1007/s12237-010-9362-6, 2011.

Lattaud, J., Lo,L., Zeeden, C., Liu, Y.-J., Song, S.-R., van der Meer, M. T. J., Damsté, J. S. S., and Schouten, S.: A multiproxy study of past environmental changes in the Sea of Okhotsk during the last 1.5 Ma, Org. Geochem., 132, 50–61, https://doi.org/10.1016/j.orggeochem.2019.04.003, 2019.

Lembke-Jene, L., Tiedemann, R., Nürnberg, D., Kokfelt, U., Kozdon, R., Max, L., Röhl, U., and Gorbarenko, S. A.: Deglacial variability in Okhotsk Sea Intermediate Water ventilation and biogeochemistry: Implications for North Pacific nutrient supply and productivity, Quat. Sci. Rev., 160, 116-137, https://doi.org/10.1016/j.quascirev.2017.01.016, 2017.

Lo, L., Belt, S. T., Lattaud, J., Friedrich, T., Zeeden, C., Schouten, S., Smik, L., Timmermann, A., Cabedo-Sanz, P., Huang, J.-J., Zhou, L., Ou, T.-H., Chang, Y.-P., Wang, L.-C., Chou, Y.-M., Shen, C.-C., Chen, M.-T., Wei, K.-Y., Song, S.-R., Fang, T.-H., Gorbarenko, S. A., Wang, W.-L., Lee, T.-Q., Elderfield, H., and Hodell, D. A.: Precession and atmospheric CO_2 modulated variability of sea ice in the central Okhotsk Sea since 130,000 years ago, Earth Planet. Sc. Lett., 488, 36–45, https://doi.org/10.1016/j.epsl.2018.02.005, 2018.

Martens, J., Wild, B., Pearce, C., Tesi, T., Andersson, A., Bröder, L., O'Regan, M., Jacobsson, M., Sköld, M., Gemery, L., Cronin, T. M., Semiletov, I., Dudarev, O. V., and Gustafsson, Ö.: Remobilization of old permafrost carbon to Chukchi Sea sediments during the end of the last deglaciation, Global Biogeochem. Cy., 33, 2–14, https://doi.org/10.1029/2018GB005969, 2019.

Martens, J., Wild, B., Muschitiello, F., O'Regan, M., Jacobsson, M., Semiletov, I., Dudarev, O. V., and Gustafsson, Ö.: Remobilization of dormant carbon from Siberian-Arctic permafrost during three past warming events, Science Advances, 6, eabb6546, 2020.

Max, L., Riethdorf, J.-R., Tiedemann, R., Smirnova, M., Lembke-Jene, L., Fahl, K., Nürnberg, D., Matul, A., and Mollenhauer, G.: Sea surface temperature variability and sea-ice extent in the subarctic northwest Pacific during the past 15,000 years, Paleoceanography, 27, PA3213, https://doi.org/10.1029/2012PA002292, 2012.

Max, L., Lembke-Jene, L., Riethdorf, J.-R., Tiedemann, R., Nürnberg, D., and Mackensen, A.: Pulses of enhanced North Pacific Intermediate Water ventilation from the Okhotsk Sea and Bering Sea during the last deglaciation, Clim. Past, 10, 591–605, https://doi.org/10.5194/cp-10-591-2014, 2014.

Méheust, M., Stein, R., Fahl, K., Max, L., and Riethdorf, J. R.: High-resolution IP_{25}-based reconstruction of sea-ice variability in the western North Pacific and Bering Sea during the past 18,000 years, Geo-Mar. Lett., 36,101–111, https://doi.org/10.1007/s00367-015-0432-4, 2016.

Méheust, M., Stein, R., Fahl, K., and Gersonde, R.: Sea-ice variability in the subarctic North Pacific and adjacent Bering Sea during the past 25 ka: new insights from IP_{25} and $U^{k'}_{37}$ proxy records, Arktos, 4, 1–19, https://doi.org/10.1007/s41063-018-0043-1, 2018.

Meyer, V. D., Max, L., Hefter, J., Tiedemann, R., and Mollenhauer, G.: Glacial-to-Holocene evolution of sea surface temperature and surface circulation in the subarctic northwest Pacifific and the Western Bering Sea, Paleoceanography, 31, 916–927, https://doi.org/10.1002/2015PA002877, 2016.

Meyer, V. D., Hefter, J., Lohmann, G., Max, L., Tiedemann, R., and Mollenhauer, G.: Summer temperature evolution on the Kamchatka Peninsula, Russian Far East, during the past 20 000 years, Clim. Past, 13, 359–377, https://doi.org/10.5194/cp-13-359-2017, 2017.

Meyer, V. D., Hefter, J., Köhler, P., Tiedemann, R., Gersonde, R., Wacker, L., and Mollenhauer, G.: Permafrost-carbon mobilization in Beringia caused by deglacial meltwater runoff, sea-level rise and warming, Environ. Res. Lett., 14, 085003, https://doi.org/10.1088/1748-9326/ab2653, 2019.

Morley, J. J., Heusser, L. E., and Shackleton, N. J.: Late Pleistocene/Holocene radiolarian and pollen records from sediments in the Sea of Okhotsk, Paleoceanography, 6, 121–131, https://doi.org/10.1029/90PA02031, 1991.

Nakatsuka, T., Toda, M., Kawamura, K., and Wakatsuchi, M.: Dissolved and particulate organic carbon in the Sea of Okhotsk: Transport from continental shelf to ocean interior, J. Geophys. Res., 109, C09S14, https://doi.org/10.1029/2003JC001909, 2004.

Praetorius, S. K., Mix, A. C., Walczak, M. H., Wohowe, M. D., Addison, J. A., and Prahl, F. G.: North Pacific deglacial hypoxic events linked to abrupt ocean warming, Nature, 527, 362–366, https://doi.org/10.1038/nature15753, 2015.

Rasmussen, S. O., Seierstad, I. K., Andersen, K. K., Bigler, M., Dahl-Jensen, D., and Johnsen, S. J.: Synchronization of the NGRIP, GRIP, and GISP2 ice cores across MIS 2 and palaeoclimatic implications, Quaternary Sci. Rev., 27, 18–28, https://doi.org/10.1016/j.quascirev.2007.01.016, 2008.

Riethdorf, J.-R., Max, L., Nürnberg, D., Lembke-Jene, L., and Tiedemann, R.: Deglacial history of (sub) sea surface temperatures and salinity in the subarctic NW Pacifific: implications for upper-ocean stratification, Paleoceanography 28, 91e104, https://doi.org/10.1002/palo.20014, 2013.

Schirrmeister, L., Froese, D., Tumskoy, V., Grosse, G., and Wetterich, S.: Yedoma: Late Pleistocene ice-rich syngenetic permafrost of Beringia, in: Encyclopedia of Quaternary Science (second edition), edited by: Elias, S. A. and Mock, C. J., Elsevier., Amsterdam, 542–552, https://doi.org/10.1016/B978-0-444-53643-3.00106-0, 2013.

Schuur, E. A. G., McGuire, A. D., Schädel, C., Grosse, G., Harden, J. W., Hayes, D. J., Hugelius, G., Koven, C. D., Kuhry, P., Lawrence, D. M., Natali, S. M., Olefeld, D., Romanovsky, V. E., Schaefer, K., Turetsky, M. R., Treat, C. C., and Vonk, J. E.: Climate change and the permafrost carbon feedback, Nature, 520, 171–179, https://doi.org/10.1038/nature14338, 2015.

Schweger, C., Froese, D., White, J. M., and Westgate, J. A.: Pre-glacial and interglacial pollen records over the last 3 Ma from northwest Canada: Why do Holocene forests differ from those of previous interglaciations?, Quaternary Sci. Rev., 30, 2124–2133. https://doi.org/10.1016/j.quascirev.2011.01.020, 2011.

Seki, O., Harada, N., Sato, M., Kawamura, K., Ijiri, A., and Nakatsuka, T.: Assessment for paleoclimatic utility of terrestrial biomarker records in the Okhotsk Sea sediments, Deep-Sea Res. Pt. II, 85–92, https://doi.org/10.1016/j.dsr2.2011.03.008, 2012.
Seki, O., Mikami, Y., Nagao, S., Bendle, J.A., Nakatsuka, T., Kim, V. I., Shesterkin, V. P., Makinov, A. N., Fukushima, M., Mossen, H. M., and Schouten, S.: Lignin phenols and BIT index distribution in the Amur River and the Sea of Okhotsk: Implications for the source and transport of particulate terrestrial OC to the Ocean, Prog. Oceanogr., 126, 146–154, http://dx.doi.org/10.1016/j.pocean.2014.05.003, 2014.
Strauss, J., Laboor, S., Schirrmeister, L., Fedorov, A. N., Fortier, D., Froese, D., Fuchs, M., Günther, F., Grigoriev, M., Harden, J., Hugelius, G., Jongejans, L. L., Kanevskiy, M., Kholodov, A., Kunitsky, V., Kraev, G., Lozhkin, A., Rivkina, E., Shur, Y., Siegert, C., Spektor, V., Streletskaya, I., Ulrich, M., Vartanyan, S., Veremeeva, A., Anthony, K. W., Wetterich, S., Zimov, N., and Grosse, G.: Circum-Arctic Map of the Yedoma Permafrost Domain, Front. Earth Sci., 9:758360. https://doi.org/10.3389/feart.2021.758360, 2021.
Sun, S., Schefuβ, E., Mulitza, S., Chiessi, C. M., Sawakuchi, A. O., Zabel, M., Baker, P. A., Hefter, J., and Mollenhauer, G.: Origin and processing of terrestrial organic carbon in the Amazon system: lignin phenols in river, shelf, and fan sediments, Biogeosciences, 14, 2495–2512. https://doi.org/10.5194/bg-14-2495-2017, 2017.
Tarasov, P. E., Bezrukova, E. V., and Krivonogov, S. K.: Late Glacial and Holocene changes in vegetation cover and climate in southern Siberia derived from a 15 kyr long pollen record from Lake Kotokel, Clim. Past, 5, 285–295, https://doi.org/10.5194/cp-5-285-2009, 2009.
Tesi, T., Semiletov, I., Hugelius, G., Dudarev, O., Kuhry, P., and Gustafsson, Ö.: Composition and fate of terrigenous organic matter along the Arctic land-ocean continuum in East Siberia: Insights from biomarkers and carbon isotopes, Geochim. Cosmochim. Ac., 133, 235–256, http://dx.doi.org/10.1016/j.gca.2014.02.045, 2014.
Tesi, T., Muschitiello, F., Smittenberg, R. H., Jakobsson, M., Vonk, J. E., Hill, P., Andersson, A., Kirchner, N., Noormets, R., Dudarev, O., Semiletov, I., and Gustafsson, Ö.: Massive remobilization of permafrost carbon during post-glacial warming, Nature Commun., 7, 13653, https://doi.org/10.1038/ncomms13653, 2016.
Vaks, A., Gutareva, O. S., Breitenbach, S. F. M., Avirmed, E., Mason, A. J., Thomas, A. L., Osinzev, A. V., Kononov, A. M., and Henderson, G. M.: Speleothems Reveal 500,000-year history of Siberian Permafrost, Science, 340, 183–186, 2013.
Vaks, A., Mason, A. J., Breitenbach, S. F. M., Kononov, A. M., Osinzev, A. V., Rosensaft, M., Borshevsky, A., Gutareva, O. S., and Henderson, G. M.: Palaeoclimate evidence of vulnerable permafrost during times of low sea ice, Nature, 577, 221–225, https://doi.org/10.1038/s41586-019-1880-1, 2020.
Vandenberghe, J., Renssen, H., Roche, D. M., Goosse, H., Velichko, A. A., Gorbunov, A., and Levavasseur, G.: Eurasian permafrost instability constrained by reduced sea-ice cover, Quaternary Sci. Rev., 34, 16–23, https://doi.org/10.1016/j.quascirev.2011.12.001, 2012.
Vandenberghe, J., French, H. M., Gorbunov, A., Marchenko, S., Velichko, A. A., Jin, H., Cui, Z., Zhang, T., and Wan, X.: The Last Permafrost Maximum (LPM) map of the Northern Hemisphere: permafrost extent and mean annual air temperatures, 25–17 ka BP, Boreas, 43, 652–666, https://doi.org/10.1111/bor.12070, 2014.
Walter Anthony, K. M., Zimov, S. A., Grosse, G., Jones, M. C., Anthony, P. M., Chapin III, F. S., Finlay, J. C., Mack, M. C., Davydov, S., Frenzel, P., and Frolking, S.: A shift of thermokarst lakes from carbon sources to sinks during the Holocene epoch, Nature, 511, 452–456, https://doi.org/10.1038/nature13560, 2014.
Walter, K. M., Zimov, S. A., Chanton, J. P., Verbyla, D., and Chapin III, F. S.: Methane bubbling from Siberian thaw lakes as a positive feedback to climate warming, Nature, 443, 71–75, https://doi.org/10.1038/nature05040, 2006.
Walter, K. M., Edwards, M. E., Grosse, G., Zimov, S. A., and Chapin III, F. S.: Thermokarst lakes as a source of atmospheric CH_4 during the last deglaciation, Science, 318, 633–636, https://doi.org/10.1126/science.1142924, 2007.
Wang, R., Kuhn, G., Gong, X., Biskabrn, B. K., Gersonde, R., Lembke-Jene, L., Lohmann, G., Tiedemann, R., and Diekmann, B.: Deglacial land-ocean linkages at the Alaskan continental

margin in the Bering Sea, Front. Earth Sci., 9:712415, https://doi.org/10.3389/feart.2021.712415, 2021.

Winterfeld, M., Goñi, M. A., Just, J., Hefter, J., and Mollenhauer, G.: Characterization of particulate organic matter in the Lena River delta and adjacent nearshore zone, NE Siberia-Part 2: Lignin-derived phenol compositions, Biogeosciences, 12, 2261–2283, https://doi.org/10.5194/bg-12-2261-2015, 2015.

Winterfeld, M., Mollenhauer, G., Dummann, W., Köhler, P., Lembke-Jene, L., Meyer, V. D., Hefter, J., Mclntyre, C., Wacker, L., Kokfelt, U., and Tiedemann, R.: Deglacial mobilization of pre-aged terrestrial carbon from degrading permafrost, Nature Commun., 9, 3666, https://doi.org/10.1038/s41467-018-06080-w, 2018.

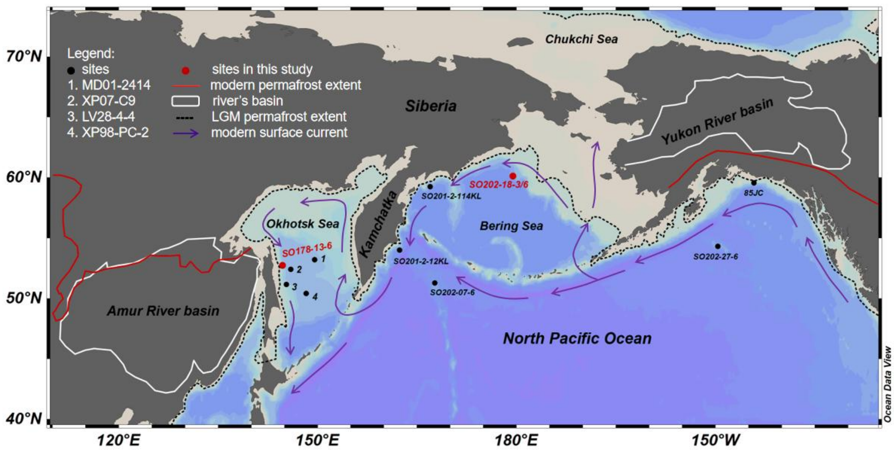

Figure 1. Study area. Red dots indicate locations of sediment cores investigated in this study; black dots denote cores described in previous studies. 1: site MD01-2414 (Lattaud et al., 2019; Lo et al., 2018). 2: site XP07-C9 (Seki et al., 2012). 3: site LV28-4-4 (Winterfeld et al., 2018). 4: site XP98-PC-2 (Seki et al., 2014).

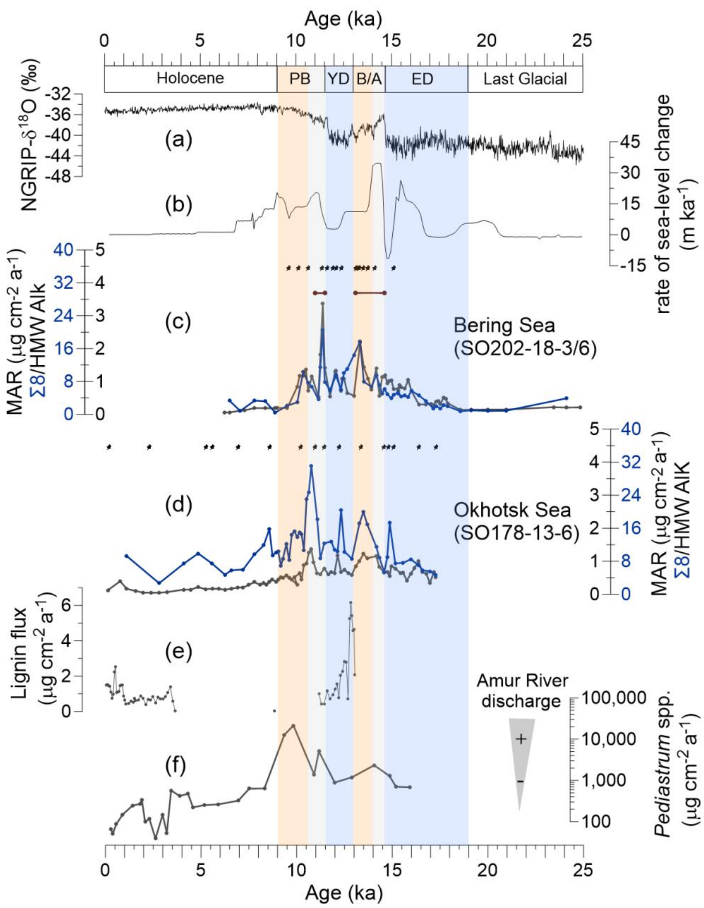

Figure 2. Proxy records of terrestrial organic matter supply and environmental records of deglacial changes. (a) Greenland NGRIP $\delta^{18}O$ (Rasmussen et al., 2008). (b) Global rate of sea-level change (Lambeck et al., 2014). (c) MAR of lignin phenols (blue) and HMW Alk (black; Meyer et al., 2019) from core SO202-18-3/6. (d) MAR of lignin phenols (blue) and HMW Alk (black; Winterfeld et al., 2018) from core SO178-13-6. Pin marks at the top of (c) and (d) show age control points, the accelerator mass spectrometry ^{14}C dates for SO202-18-3/6 (Kuehn et al., 2014) and SO178-13-6 (Max et al., 2012). Brown bars in panel c indicate laminated/layered (anoxic) core sections (Kuehn et al., 2014). (e) Lignin flux from core 4-PC1 (Chukchi Sea, Martens et al., 2019). (f) Accumulation rate of chlorophycean freshwater algae *Pediastrum* spp. from core LV28-4-4 (Winterfeld et al., 2018). Blue boxes represent the cold spells the early deglaciation (ED) and Younger Dryas (YD), orange boxes are for the warm phases Bølling-Allerød (B/A) and Pre-Boreal (PB). Gray boxes highlight the periods of melt water pulse 1A (MWP-1A) and 1B (MWP-1B).

https://doi.org/10.5194/cp-2022-67
Preprint. Discussion started: 6 September 2022

Climate of the Past
Discussions
Open Access

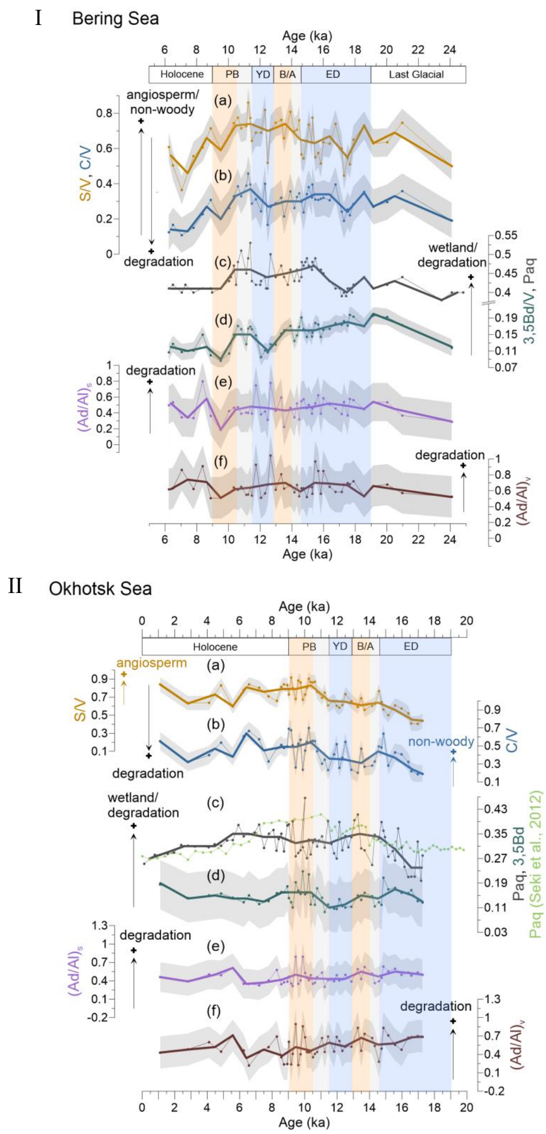

Figure 3. Records of lignin indices compared with the HMW Alk and Paq index in Bering and Okhotsk Sea sediments. (a and b): S/V and C/V ratios reflect the vegetation change and/or degree of lignin degradation in the respective river basins. (c and d): 3,5Bd/V and Paq ratios represent the wetland extent or degree of degradation in the respective catchments. In the Okhotsk Sea record, the light green line represents the Paq of a nearby core, XP07-C9 (Seki et al., 2012). (e and f): The Ad/Al can reflect the degradation of lignin phenols. Grey shaded areas illustrate the uncertainty of these indices. Bold lines are the 1 ka averages of the corresponding indices. Blue boxes represent the cold spells the early deglaciation (ED) and Younger Dryas (YD), orange boxes are for the warm phases Bølling-Allerød (B/A) and Pre-Boreal (PB). Gray boxes highlight the periods of melt water pulse 1A (MWP-1A) and 1B (MWP-1B).

https://doi.org/10.5194/cp-2022-67
Preprint. Discussion started: 6 September 2022

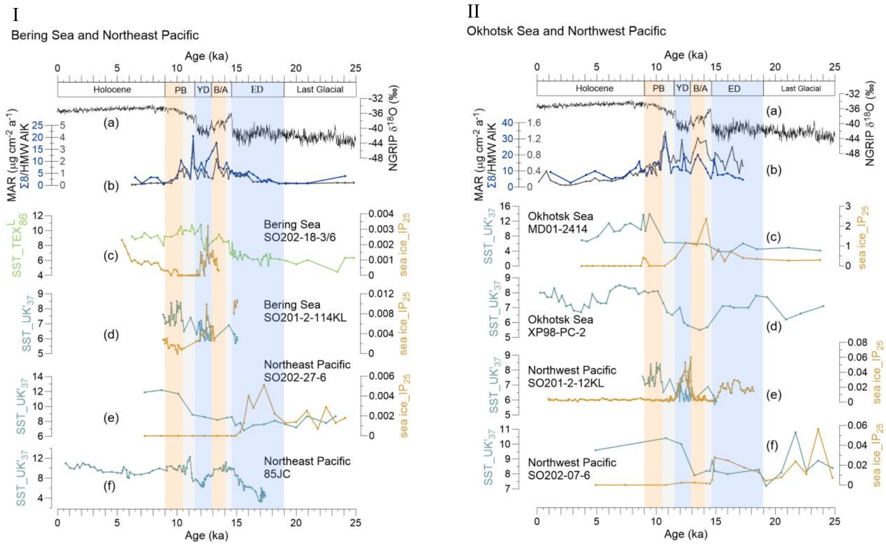

Figure 4. Records of sea surface temperature (SST) and sea ice (IP_{25}) in the Bering Sea and Northeast Pacific, and Okhotsk Sea and Northwest Pacific during the past 25 ka. (a) The NGRIP-$\delta^{18}O$ of the Greenland (Rasmussen et al., 2008). (b) The MAR of biomarkers.
I: (c) Light green line is the SST (TEX^{L}_{86}) of this study, SO202-18-3/6. The brown line is the IP_{25} of this core (Méheust et al., 2018). (d) SST and IP_{25} of the core SO202-2-114KL (Max et al., 2012; Méheust et al., 2016). (e) SST and IP_{25} of the core SO202-27-6 in the Northeast Pacific (Méheust et al., 2018). (f) SST of the core 85JC (Praetorius et al., 2015).
II: (c) SST and IP_{25} of the core MD01-2414 in the Okhotsk Sea (Lattaud et al., 2019; Lo et al., 2018). (d) SST of the core XP98-PC-2 (Seki et al., 2014). (e) SST and IP_{25} of the core SO201-2-12KL in the Northwest Pacific (Max et al., 2012; Méheust et al., 2016). (f) SST and IP_{25} of the core SO202-07-6 (Méheust et al., 2018). The units of the SST and IP_{25} are °C and $\mu g\ g^{-1}$ sediment, respectively. Blue boxes represent the colder conditions during the early deglaciation (ED) and Younger Dryas (YD) cold spell, orange boxes are for the warm phases Bølling-Allerød (B/A) and Preboreal (PB). Gray boxes highlight the periods of melt water pulse 1A (MWP-1A) and 1B (MWP-1B).

https://doi.org/10.5194/cp-2022-67
Preprint. Discussion started: 6 September 2022

Climate of the Past
Discussions
Open Access

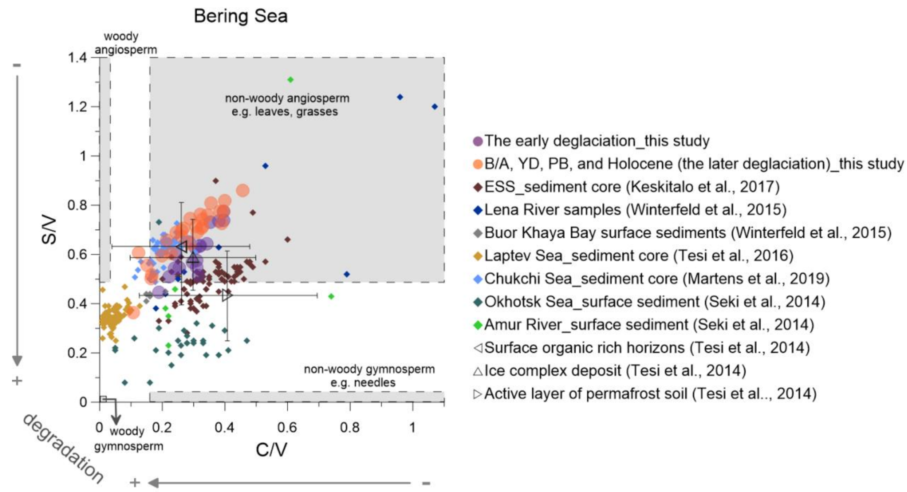

Figure 5. Lignin indicators of terrigenous material in the Bering sediment (solid circles) compared with previously studied (Martens et al., 2019; Keskitalo et al., 2017; Tesi et al., 2016; Seki et al., 2014; Winterfeld et al., 2015). The early deglaciation is from 19 to 14.6 ka BP and after the early deglaciation is the later deglaciation. The dark triangles represent the ratio of S/V and C/V from surface soils, Ice Complex deposits and active layer permafrost (Tesi et al., 2014). ESS is short for the East Siberian Shelf.

https://doi.org/10.5194/cp-2022-67
Preprint. Discussion started: 6 September 2022

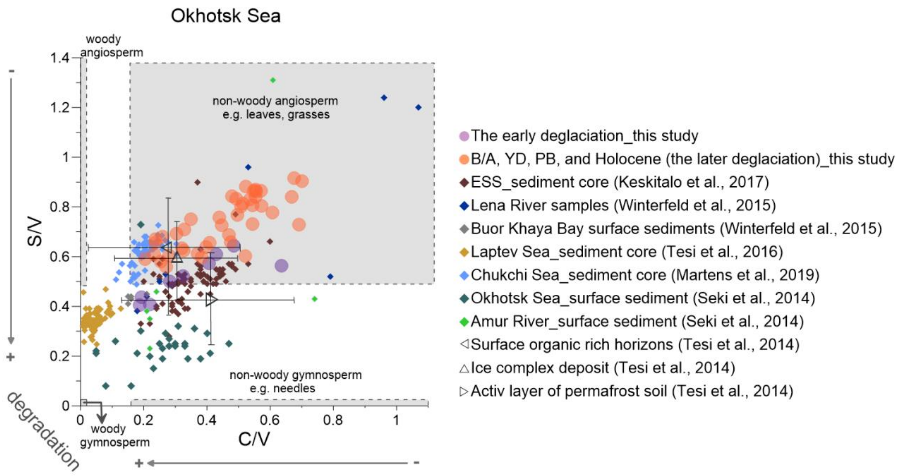

Figure 6. Lignin indicators of terrigenous material in the Okhotsk Sea sediment (solid circles) compared with previously studied (Martens et al., 2019; Keskitalo et al., 2017; Tesi et al., 2016; Seki et al., 2014; Winterfeld et al., 2015). The early deglaciation is from 19 to 14.6 ka BP and after the early deglaciation is the later deglaciation. The dark triangles represent the ratio of S/V and C/V from surface soils, Ice Complex deposits and active layer permafrost (Tesi et al., 2014). ESS is short for the East Siberian Shelf.